AD-A115 867 ROCKWELL INTERNATIONAL THOUSAND OAKS CA ELECTRONICS--ETC F/G 17/5
DEVELOPMENT OF CHARGE TRANSFER DEVICES FOR 1-2 MICRON IMAGING.(U)
MAR 81 R A MILANO, Y Z LIU, R J ANDERSON DAAK70-79-C-0145
UNCLASSIFIED ERC41034.27FR NL

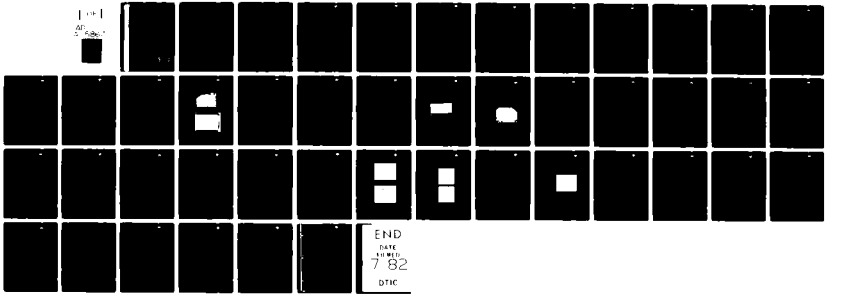

(12)

27

Report ERC41034.27FR

Development of Charge Transfer Devices for 1-2 Micron Imaging

R.A. Milano, Y.Z. Liu, Robert J. Anderson and Marshall J. Cohen
Rockwell International
Microelectronics Research and Development Center
1049 Camino Dos Rios
Thousand Oaks, California 91360

March, 1981

Final Report for Period 09/06/79 through 01/31/81

"Unclassified" Approved for public release.

Prepared for

W26P7Z
Director
Night Vision/Electro Optics Lab
Fort Belvoir, VA 22060

UNCLASSIFIED

SECURITY CLASSIFICATION OF THIS PAGE (When Data Entered)

REPORT DOCUMENTATION PAGE	READ INSTRUCTIONS BEFORE COMPLETING FORM
1. REPORT NUMBER	2. GOVT ACCESSION NO. AD-A115864	3. RECIPIENT'S CATALOG NUMBER
4. TITLE (and Subtitle) Development of Charge Transfer Devices for 1-2 Micron Imaging	5. TYPE OF REPORT & PERIOD COVERED Final Report 09/06/79 to 01/31/81
	6. PERFORMING ORG. REPORT NUMBER ERC41034.27FR
7. AUTHOR(s) R.A. Milano, Y.Z. Liu, Robert J. Anderson and Marshall J. Cohen	8. CONTRACT OR GRANT NUMBER(s) DAAK70-79-C-0145
9. PERFORMING ORGANIZATION NAME AND ADDRESS Rockwell International Microelectronics Research and Development Center 1049 Camino Dos Rios, Thousand Oaks, CA. 91360	10. PROGRAM ELEMENT, PROJECT, TASK AREA & WORK UNIT NUMBERS
11. CONTROLLING OFFICE NAME AND ADDRESS W26P7Z Director Night Vision/Electro Optics Lab Fort Belvoir, VA. 22060	12. REPORT DATE March, 1981
	13. NUMBER OF PAGES 40
14. MONITORING AGENCY NAME & ADDRESS(if different from Controlling Office)	15. SECURITY CLASS. (of this report) Unclassified
	15a. DECLASSIFICATION/DOWNGRADING SCHEDULE

16. DISTRIBUTION STATEMENT (of this Report)

"Unclassified: Approved for public release."

17. DISTRIBUTION STATEMENT (of the abstract entered in Block 20, if different from Report)

18. SUPPLEMENTARY NOTES

19. KEY WORDS (Continue on reverse side if necessary and identify by block number)

CCD
CCD Imager
Infrared imaging
GaSb

LAMBDA > 6V = 0.99 MICROMETERS

20. ABSTRACT (Continue on reverse side if necessary and identify by block number)

Currently no satisfactory solid state imaging device exists for use in near infrared applications. While transmission photocathodes are most often used, their spectral response rapidly falls off for $\lambda \geq 0.99$ μm due to the minimum vacuum level which can be achieved with a cesiated III-V semiconductor surface. These devices are thus suitable for use in those night vision systems which operate in the visible or near-infrared spectrum under low level moonlight and starlight illumination. They are, however, ineffective under moonless or overcast conditions because of the lack of light in the 0.5-0.9 μm region. A

DD FORM 1 JAN 73 1473 EDITION OF 1 NOV 65 IS OBSOLETE

UNCLASSIFIED

SECURITY CLASSIFICATION OF THIS PAGE (When Data Entered)

heterojunction imaging charge coupled device, CCD, in the GaSb-AlGaAsSb material system would eliminate the vacuum level problem and make possible the design and construction of imagers whose long wavelength cut-off is $\geq 1.8\mu m$. Since there is considerable night glow ambient illumination in the 1.0-1.8 μm wavelength region, this device is ideally suited to night vision applications.

This program focused on the development of a backside illuminated, imaging, heterojunction CCD. This program is the forerunner of an analogous concept currently employed in the design of AlGaAs/GaAs imaging devices and great success has been achieved. The CCD consists of three layers and is permanently bonded to a glass substrate. Metallization patterns which define the device active area and individual pixels are fabricated on the top, AlGaAsSb, n-type channel layer. Charge storage and transfer take place in this layer. The alloy composition is adjusted to maximize the bandgap resulting in low dark current. This n-AlGaAsSb layer and another (p-type) AlGaAsSb "window" layer, together sandwich the GaSb optical absorber. Thus, light penetrates the glass and the transparent window layer and is strongly absorbed in the GaSb layer. Photogenerated electrons diffuse to the p+-n junction, where they are swept into potential wells in the channel. In addition to the optimal spectral response and low dark current, the device has high optical quantum efficiency, is radiation hard, and naturally anti-blooming owing to the Schottky barrier transfer gates and has a wide dynamic range.

The primary objective of this contract was the successful fabrication and operation of a charge coupled device made in AlGaAsSb. In order to accomplish this goal, the basic elements of the device, i.e., materials properties, characteristics of the Schottky barrier diodes and ohmic contacts, had to be analyzed in detail. While the primary goal was not achieved, significant advantages were made in understanding the characteristics of both the material and associated devices.

The major accomplishments of this program included:

Development of a reliable ohmic contact technology,

Identification of thermally stable Schottky metallization,

Improved lattice-matching by increasing As content,

Initiation of investigation of differential wet chemical etchants.

TABLE OF CONTENTS

		Page
1.0	INTRODUCTION	1
2.0	MATERIALS GROWTH	4
3.0	SCHOTTKY BARRIERS TO AlGaAsSb	16
4.0	OHMIC CONTACTS	25
5.0	PROCESSING ISSUES	35
6.0	RECOMMENDATIONS AND CONCLUSIONS	38
	REFERENCES	40

LIST OF ILLUSTRATIONS

Page

Fig. 1. Backside-illuminated Schottky barrier gate AlGaAsSb/GaSb heterojunction CCD..... 2

Fig. 2. Temperature-time profile of the LPE growth cycle of $Al_xGa_{1-x}As_{1-y}Sb_y$..... 6

Fig. 3. Atomic fraction of Te required in the melt to achieve $N_D \approx 1 \times 10^{16} cm^{-3}$ for selected composition of $Al_xGa_{1-x}As_{1-y}Sb_y$.... 8

Fig. 4. C-V plot and Te-doping profile of a $Al_xGa_{1-x}As_{1-y}Sb_y$ ($x \sim 0.3$, $y \sim 0.99$) epitaxial layer..... 9

Fig. 5. (a) As-grown surface of AlGaSb epilayer, (b) As-grown surface of an AlGaAsSb epilayer.....10

Fig. 6. X-ray double crystal diffractometer measurement of the lattice mismatch between an AlGaAsSb epilayer and the GaSb substrates; $\Delta a_o/a_o = 0.012\%$.....11

Fig. 7. Lattice mismatch vs. atomic fraction of As in the melt for AlGaAsSb containing 20 mole percent of Al.....12

Fig. 8. Cleaved and stained cross-section of a GaSb-AlGaAsSb structure. The uniform deposition of GaSb n^+-layer onto the AlGaAsSb layer is clearly evident.....14

Fig. 9. Photograph of the as-grown surface of the wafer whose cross-section is shown in Fig. 8.....15

Fig. 10 Forward I-V characteristics of a Au-$Al_{.3}Ga_{.7}As_{.01}Sb_{.99}$ Schottky barrier diode.....18

Fig. 11. Reverse I-V characteristics of a Au-$Al_{.3}Ga_{.7}As_{.01}Sb_{.99}$ Schottky barrier diode.....19

Fig. 12. Au Schottky barrier height and energy gap vs. Al mole fraction. The I-V data is denoted by Δ and the spread in photoresponse data is denoted by vertical bars.....21

Fig. 13. Depth composition profile for AuGe/Pt/Au metallization determined by AES.....26

LIST OF ILLUSTRATIONS (Cont).

Page

Fig. 14. (a) I-V characteristics of aluminum contacts on n-$Al_{.3}Ga_{.7}AsSb$/p-GaSb (wafer K108d) after 200 keV Se implant at $1 \times 10^{13} cm^{-2}$ dosage, (b) at lower current scale..... 27

Fig. 15. Sample K108g, Ohmic metal - 400Å Ge/240Å Au, Implant - Kr^{+} - 300 KeV, 1×10^{14} ions/cm^2, post implant anneal - none. 28

Fig. 16. I-V characteristics of Sn/Ag/Ni metallization after 425°C alloy. Vert. scale: 20 mA/div, horiz. scale: 0.5 V/div..... 30

Fig. 17. Total resistance vs. alloy temperature of Ag-Sn-Ni metallization system on n-$Al_{.3}Ga_{.7}As_{.01}Sb_{.99}$. The contact areas are circular, having the diameters listed in the figure..... 31

Fig. 18. Depth composition profile for Sn/Ag/Ni metallization determined by AES. The data for all elements are X1. Al data have been deleted for clarity..... 32

Fig. 19. Depth composition profile for Sn/Ag/Ni metallization determined by AES. The data for all elements are X1. Al data have been deleted for clarity..... 33

1.0 INTRODUCTION

Currently no satisfactory solid state imaging device exists for use in near infrared applications. While transmission photocathodes are most often used, their spectral response rapidly fall off for $\lambda \geq 0.9\mu m$ due to the minimum vacuum level which can be achieved with a cesiated III-V semiconductor surface. These devices are thus suitable for use in those night vision systems which operate in the visible or near-infrared spectrum under low level moonlight and starlight illumination. They are, however, ineffective under moonless or overcast conditions because of the lack of light in the 0.5-0.9 μm region. A heterojunction imaging charge coupled device, CCD, in the GaSb-AlGaAsSb material system would eliminate the vacuum level problem and make possible the design and construction of imagers whose long wavelength cut-off is $\geq 1.8\ \mu m$. Since there is considerable night glow ambient illumination in the 1.0-1.8 μm wavelength region, this device is ideally suited to night vision applications.

The backside illuminated, imaging, heterojunction CCD concept as originally conceived for this program is illustrated in Fig. 1. This concept has since been employed in the design of AlGaAs/GaAs visible imaging devices also and great success has been achieved. The CCD consists of three layers, as shown, and is permanently bonded to a glass substrate. Metallization patterns which define the device active area and individual pixels are fabricated on the top, AlGaAsSb, n-type channel layer. Charge storage and transfer take place in this layer. The alloy composition is adjusted to maximize the bondgap resulting in low dark current. This n-AlGaAsSb layer and another (p-type) AlGaAsSb "window" layer, together sandwich the BaSb optical absorber. Thus, light penetrates the glass and the transparent window layer and is strongly absorbed in the GaSb layer. Photogenerated electrons diffuse to the p^+-n junction, where they are swept into potential wells in the channel. In addition to the optimal spectral response and low dark current, the device has high optical quantum efficiency, is radiation hard, and naturally anti-blooming owing to the Schottky barrier transfer gates and has a wide dynamic range.

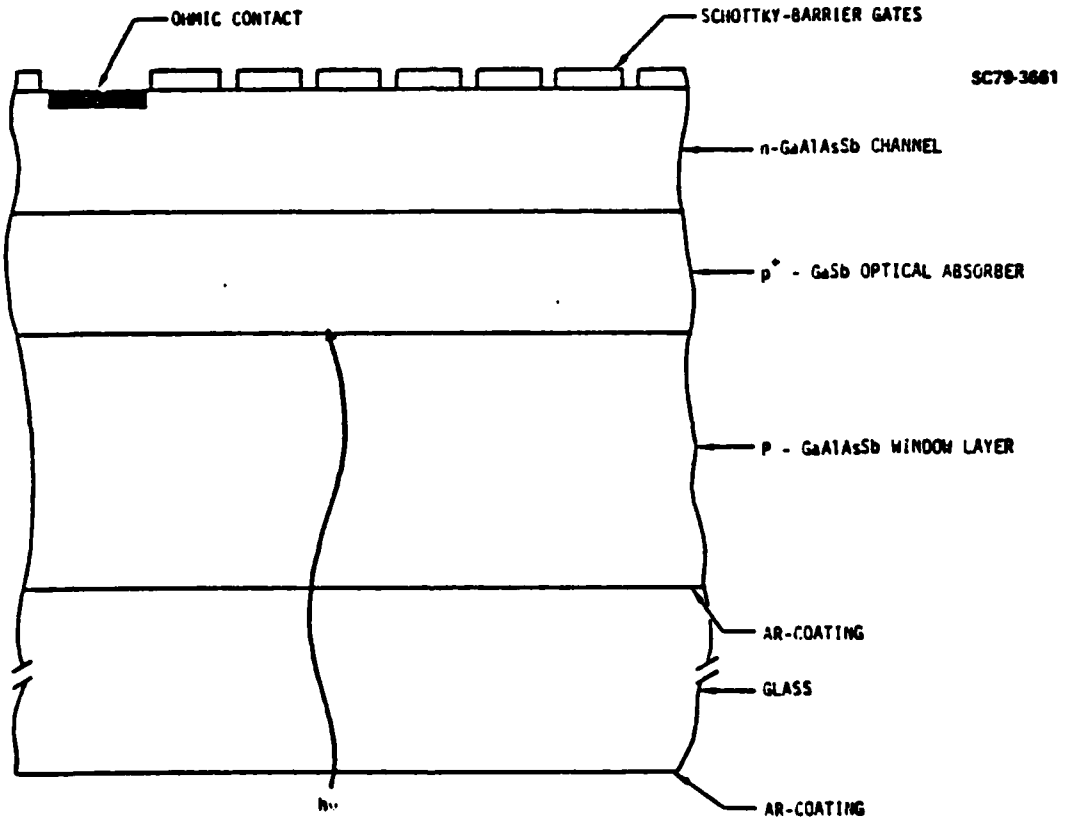

Fig. 1. Backside-illuminated Schottky barrier gate AlGaAsSb/GaSb heterojunction CCD.

The primary objective of this contract was the successful fabrication and operation of a charge coupled device made in AlGaAsSb. In order to accomplish this goal, the basic elements of the device, i.e., materials properties, characteristics of the Schottky barrier diodes and ohmic contacts, had to be analyzed in detail. While the primary goal was not achieved, significant advances were made in understanding the characteristics of both the material and associated devices.

The major accomplishments of this program included:

- Development of a reliable ohmic contact technology.
- Identification of thermally stable Schottky metallization.
- Improved lattice-matching by increasing As content.
- Initiation of investigation of differential wet chemical etchants.

These are discussed in detail in the following sections.

2.0 MATERIALS GROWTH

Although AlGaAsSb/GaSb heterostructures have been fabricated previously, more research is required in this materials system to obtain the level of maturity found in other systems, e.g., AlGaAs/GaAs, InGaAsP/InP. Of particular importance for CCD fabrication is the ability to grow multilayer structures with morphology suitable for photolithographic processing. In addition, layer thickness and doping must be well-controlled to ensure proper device operation. The ability to control the electrical and optical properties of the material over large areas is a necessity when area imagers are contemplated. The materials growth effort for this program has concentrated mainly on the following areas: (1) the elimination of misfit dislocations ("cross-hatching"), (2) determination of the optimum Al concentration for low leakage current, and (3) the investigation of the conditions required for the growth of layers of epi-material in which $X_{Al} \geq 0.3$. In addition, material was also grown for doping and layer thickness calibration and for Schottky barrier and ohmic contact studies.

The GaSb substrates used in this program were either Te doped n-type or undoped p-type (100) material. The etch pit density of the Te-doped substrate is approximately $500/cm^2$, while the undoped substrates had EPD of less than 1000. They were chemically-mechanically polished on a "kitten ear" pad with $Br\text{-}CH_3OH$ dripping on it. Due to the softness of GaSb, at least 5 mils of the material was removed by this method to remove saw-induced damage. Some of the samples were polished in fused silica gel to provide a smoother finish. Prior to growth, the substrates were again etched in $Br\text{-}CH_3OH$ to remove approximately 1 mil of the material. At times, the etch created a dull surface on the Te doped GaSb substrates. This resulted from the doping striations and did not affect the LPE growth. The Te-doped substrates were usually soaked in concentrated H_2SO_4 for 5 minutes to remove any excess Te from the surface. This is especially important for growing high purity material owing to the high distribution coefficient of Te. The substrate was then rinsed thouroughly in deionized water to remove all sulphate ions, followed by an HF soak to dissolve any residual oxides.

For the growth of AlGaAsSb of reasonably high purity ($|N_D-N_A| < 10^{15}$ cm^{-3}), a long bake of the Ga melt out at high temperature is mandatory. The gallium melt, together with the precisely measured antimony and GaAs, were baked in a purified H_2 atmosphere at 750°C for 12 hours. Figure 2 shows a typical growth schedule. Sections A, B, and C of the schedule were for baking out the melt. At D, the substrate together with the dopants and aluminum were loaded such that the aluminum was not touching the melt. The furnace was then raised to 600°C for half an hour and the aluminum was mixed with the melt. For the growth of AlGaAsSb alloys at 550°C, the growth schedule followed G_1, H_1, J_1, K_1. At H_1, the temperature of the furnace was equilibrated at ≈560°C for at least half an hour and temperature ramping started at J_1 at a rate of ½°C/min. The epitaxial layers were grown at 2-3°C supersaturation. After the growth, the furnace was quenched down to room temperature.

The channel layer of a CCD must have uniform doping and thickness for proper operation. Large fluctuations of either parameter will result in correspondingly large variations in pinch-off voltage and, hence, the clock voltage necessary for proper operation. Layer thickness is a function of the supersaturation of the melt, rate of melt cooling and total time the melt is in contact with the substrate. The contact time and cooling rate are easily controlled; however, the degree of supersaturation of the melt is subject to some variation. This results in epitaxial layers that may vary by ≅15% from the desired thickness. For the 1-2 μm thickness required for the CCD channel, this variation is not of significant concern. Layer thickness uniformity is very good over the 0.5 cm^2 substrate areas presently in use. Significant deviations from flatness are found only near the substrate perimeter and are due to the edge growth phenomena, a characteristic of the LPE growth technique.

The doping density required for a 1 μm thick CCD channel layer is N_D = 1-2 x 10^{16} cm^{-3}. Te is commonly used as an n-type dopant in the $Al_xGa_{1-x}As_{1-y}Sb_y$ system since it exhibits no amphoteric behavior. To reproducibly obtain the required doping density, the distribution coefficient of Te as a function of Al concentration must be determined. It has been found that only minute amounts of Te are needed to produce the desired N_D and that as the atomic fraction of

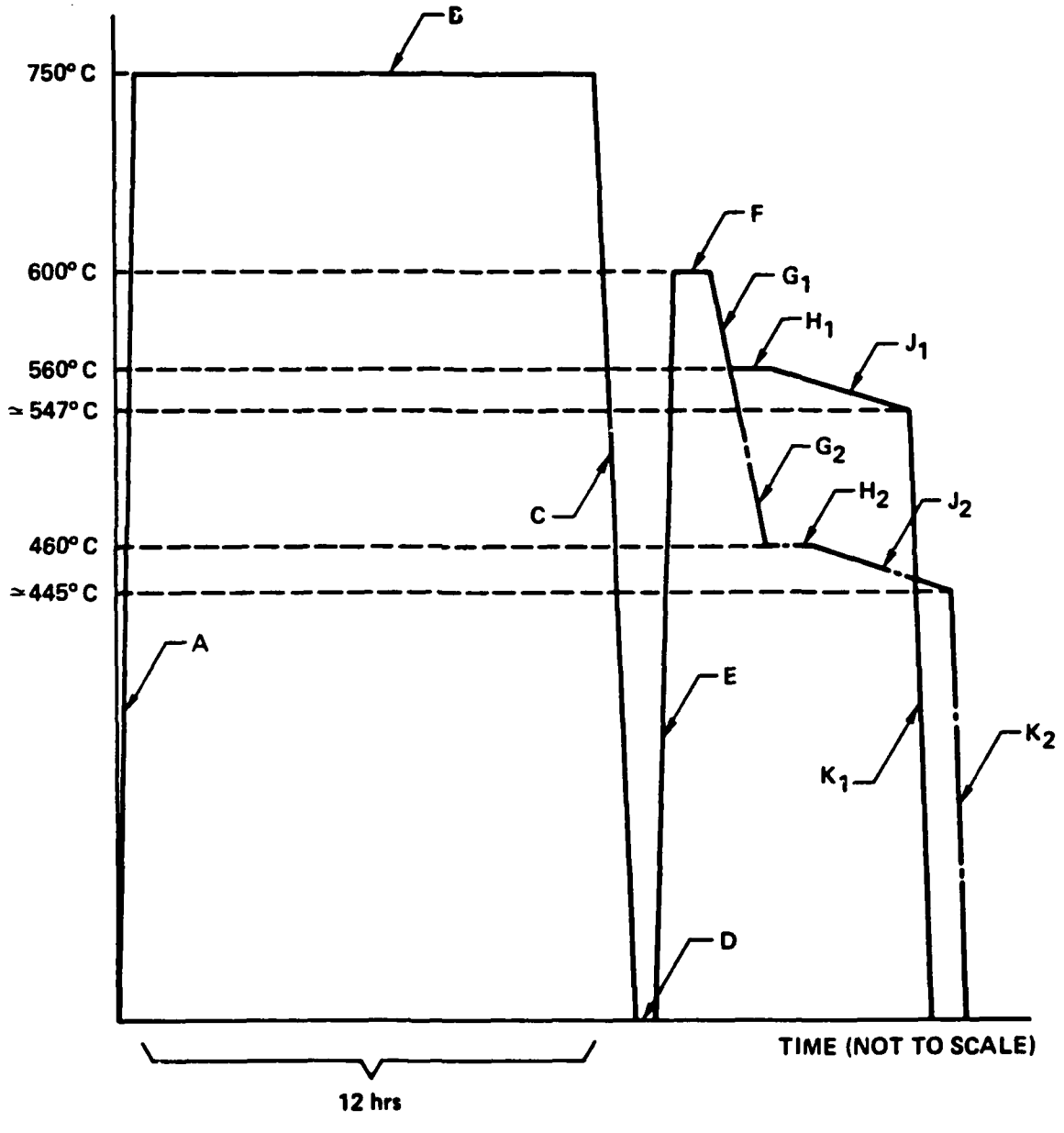

Fig. 2. Temperature-time profile of the LPE growth cycle of $Al_xGa_{1-x}As_{1-y}Sb_y$

Al in the melt (X^l_{Al}) increases, X_{Te} decreases for a fixed value of N_D. These results are summarized in Fig. 3 where X^l_{Te} for $N_D = 1 \times 10^{16}$ cm^{-3} is shown to be inversely proportional to the Al/Ga ratio in the solid (X^s_{Al}/X^s_{Ga}). Each data point represents an average value determined from several growth runs.

Differential C-V measurements were used to analyze the variation of N_D with depth in the layer. These measurements are performed on Au-Schottky barrier diodes. Typical results, shown in Fig. 4, demonstrate that N_D is very uniform throughout the layer.

The AlGaSb/GaSb materials system is similar to the AlGaAs/GaAs system in that the addition of Al will increase the bandgap while the lattice constant stays very close to that of the GaSb substrate. The percentage change in lattice constant $\Delta a/a_o$ between AlSb and GaSb is only 0.7%. While this value is small enough to permit epitaxial growth to occur, a significant number of misfit dislocations are generated. The linear density, estimated using the expression $\rho_{dl} \approx \Delta a_o/a_o^2$, is $\rho_{dl} \approx 1.6 \times 10^6$ cm^{-1}. The density of interface states in the (100) direction is $N_{ss} \sim 1.5 \times 10^{13}$ cm^{-2} ($N_{ss} \approx 8\Delta a_o/a_o^3$) which yields an unacceptably large interface recombination velocity, $S = (\sigma_t N_{ss} v_{th})$ for device applications. It is, therefore, necessary to reduce $\Delta a_o/a_o$. By adding small amounts of As to the AlGaSb melt, the lattice constant of the AlGaAsSb solid can be made to match that of the GaSb substrate. The improvement in surface morphology is shown in Fig. 5 where as-grown layers of AlGaSb(a) and AlGaAsSb(b) are compared. The results of an x-ray double crystal diffractometer measurement of the lattice mismatch of an AlGaAsSb layer on a GaSb substrate, Fig. 6, indicate that $\Delta a/a_o$ as low as 0.012% can be achieved.

In order to incorporate sufficient As into the solid to achieve lattice matching, the initial growth temperature must be ~550°C. This is due to the limited solubility of As in Al-Ga solutions. The dependence of $\Delta a/a_o$ on X^l_{As} for AlGaAsSb containing 20 mole percent Al in the solid is shown in Fig. 7. The lattice mismatch can be routinely reduced below 0.1%, yielding acceptably low values of ρ_{dl} and N_{ss} ($\rho_{dl} < 2 \times 10^4$ cm^{-1}, $N_{ss} < 2 \times 10^{12}$ cm^{-2}). The distribution coefficient of As (k_{As}) at 550°C varies with the Al content in the melt. It has been found that as the amount of Al increases, so also does k_{As}. Pertur-

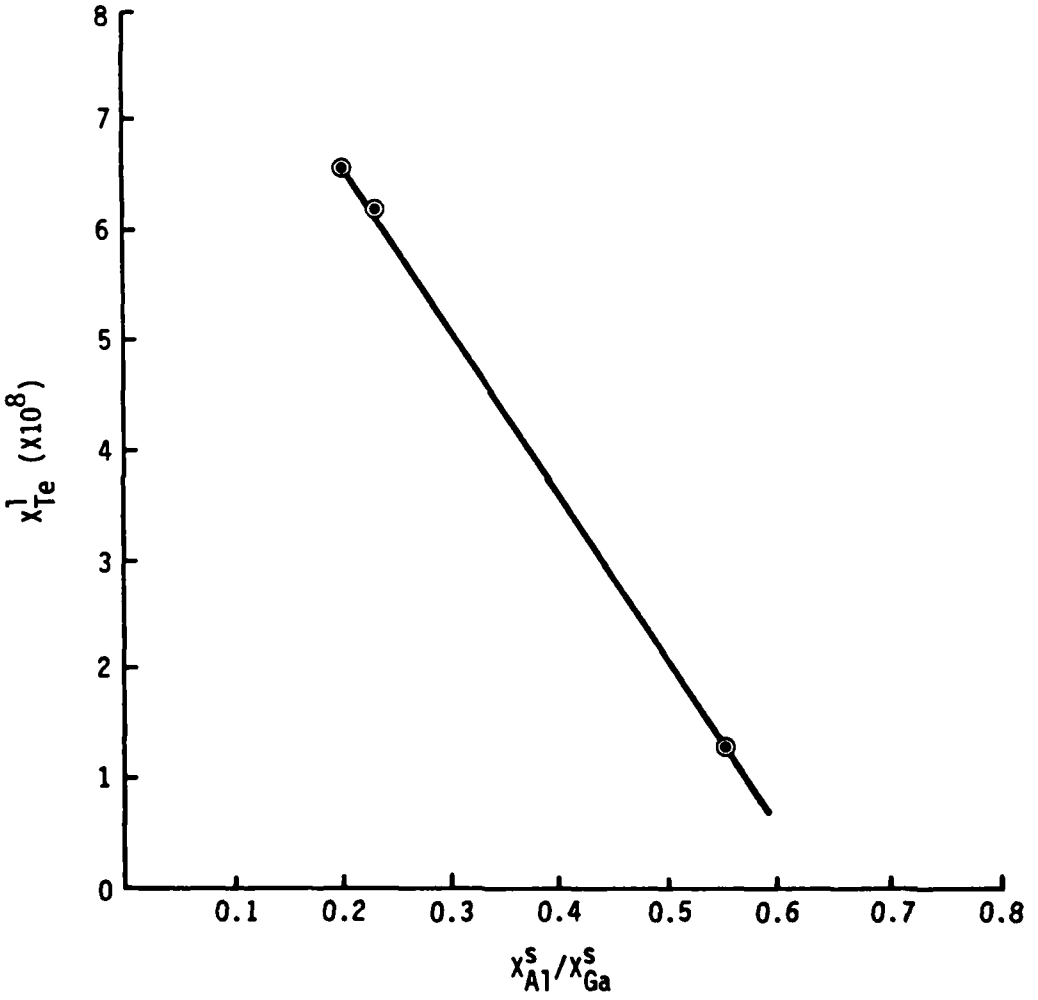

Fig. 3. Atomic fraction of Te required in the melt to achieve N_D 1 x 10^{16} cm^{-3} for selected composition of $Al_xGa_{1-x}As_{1-y}Sb_y$.

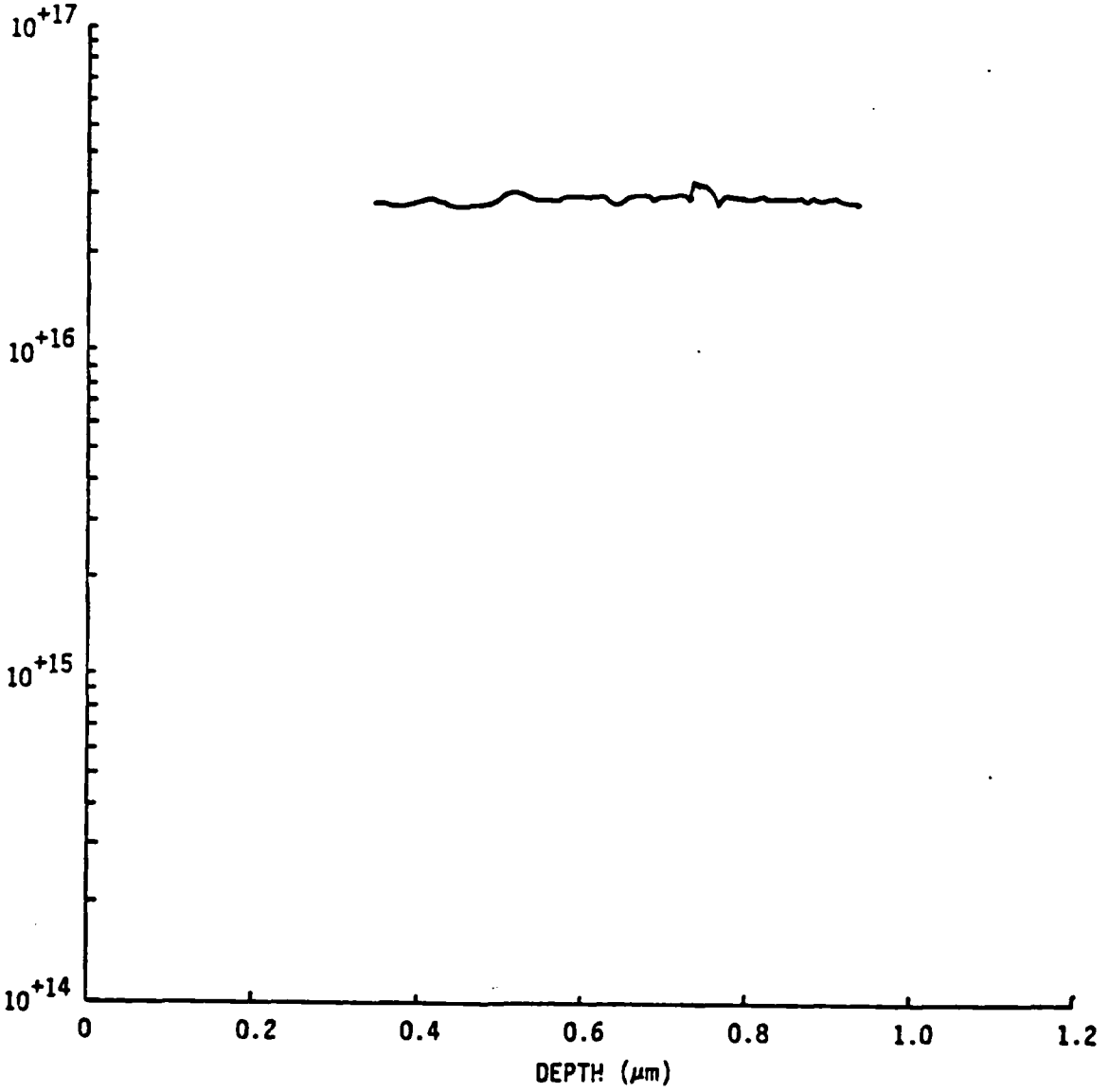

Fig. 4. C-V plot and Te-doping profile of an $Al_xGa_{1-x}As_{1-y}Sb_y$ ($x \sim 0.3$, $y \sim 0.99$) epitaxial layer.

SC79-3530

(a)

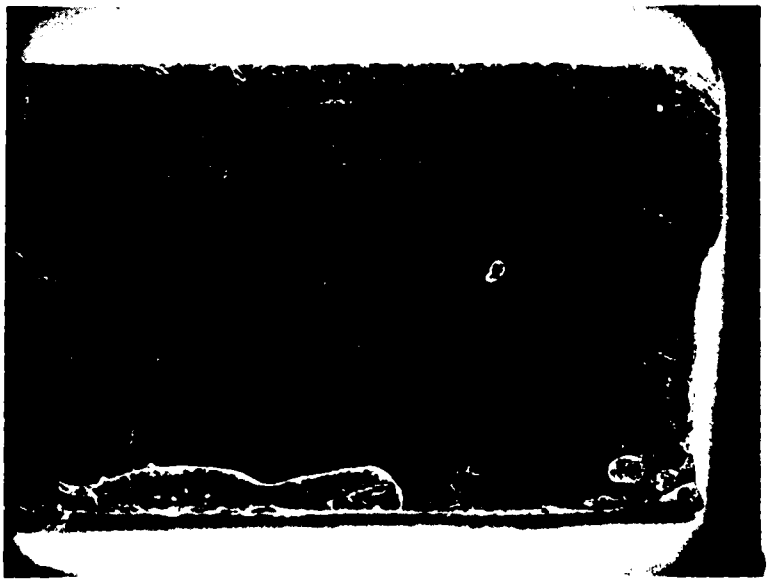

(b)

Fig. 5 (a) As-grown surface of AlGaSb epilayer, (b) As-grown surface of an AlGaAsSb epilayer.

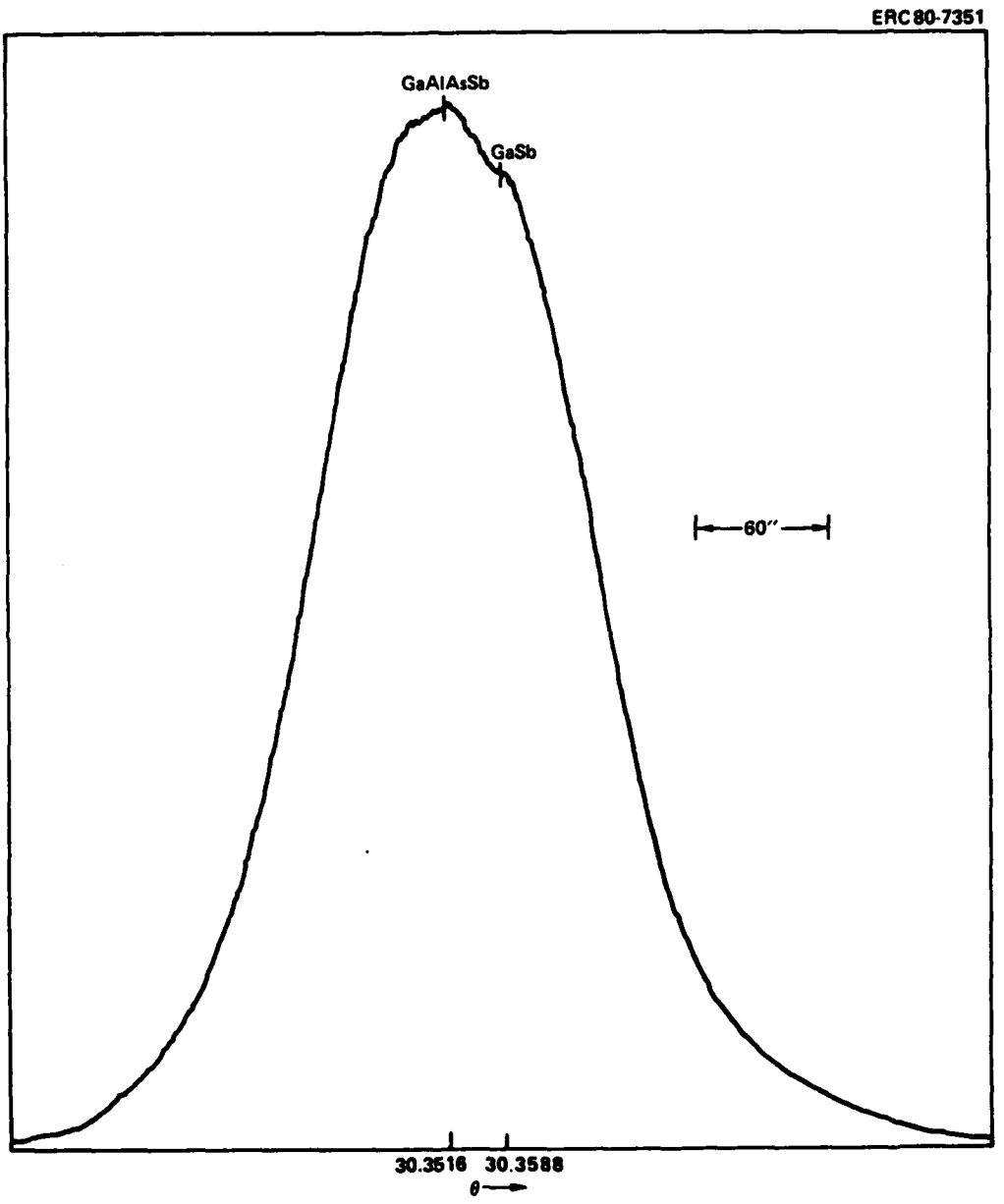

Fig. 6. X-ray double crystal diffractometer measurement of the lattice mismatch between an AlGaAsSb epilayer and the GaSb substrates; $\Delta a_o/a_o$ = 0.012%. (The Scale Marker shown in the Figure indicates the length of arc through which the reflected x-ray beam was deflected.)

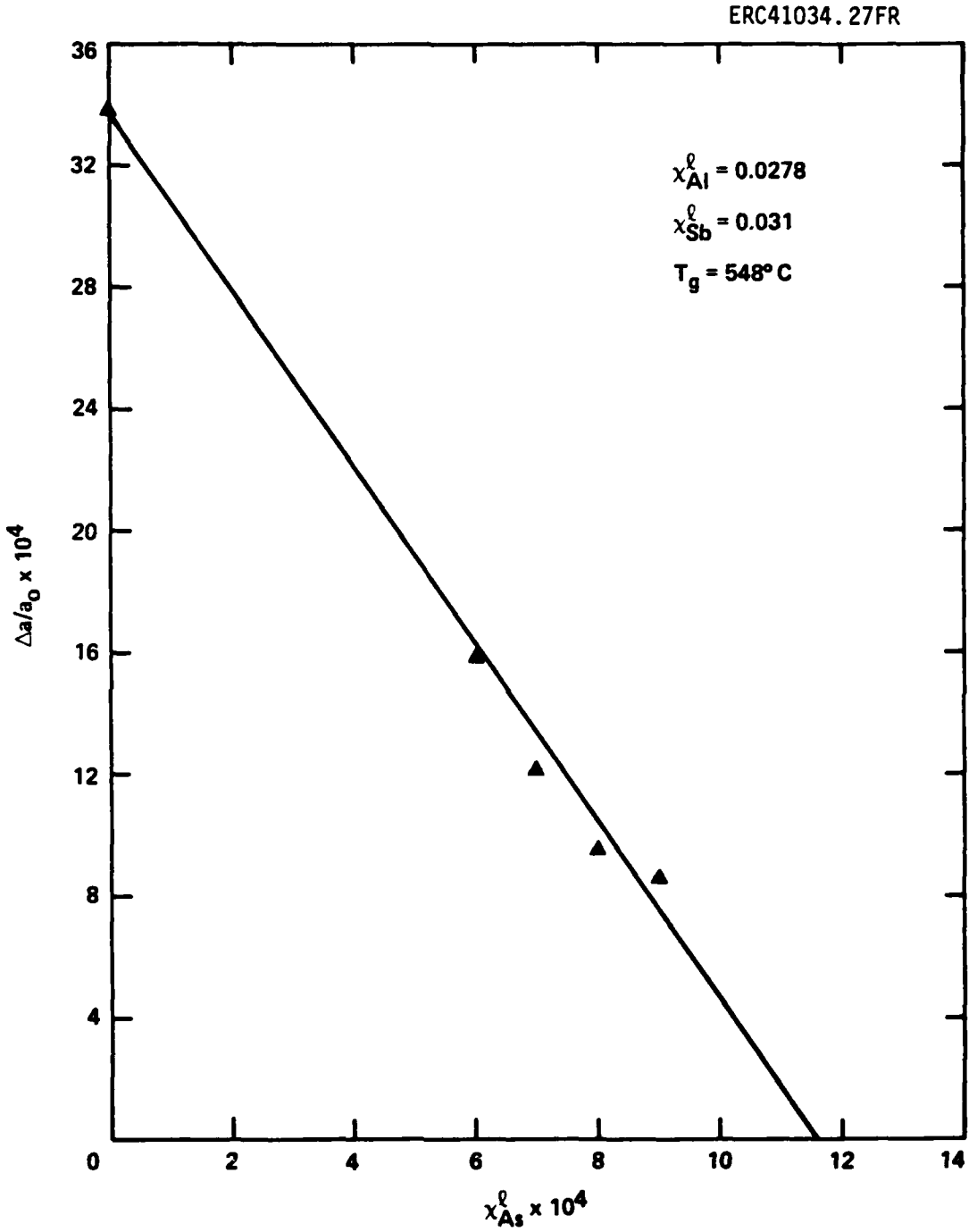

Fig. 7. Lattice mismatch vs. atomic fraction of As in the melt for AlGaAsSb containing 20 mole percent of Al.

bations of k_{As} are not uncommon and are the result of many factors including the addition of dopants to the melt.

The fabrication of a heterojunction imaging CCD structure requires a multilayer epitaxial technology in which GaSb can be grown on an already deposited quaternary layer. To ensure wetting of the GaSb to the Al bearing material, it was necessary to minimize the exposure of the freshly grown quaternary surface to the ambient gas flow, thereby minimizing the formation of surface oxides. This requires precise adjustment of the saturation temperatures of the melts so that the layers can be grown sequentially with no intervening delay. The result of this technique is shown in the cleaved and stained cross-section of Fig. 8. The dark line in the photograph is the result of a poor cleave and is not part of the original structure. Shown in Fig. 9 is the as-grown surface of this two-layer structure. Note that excellent surface morphology was maintained.

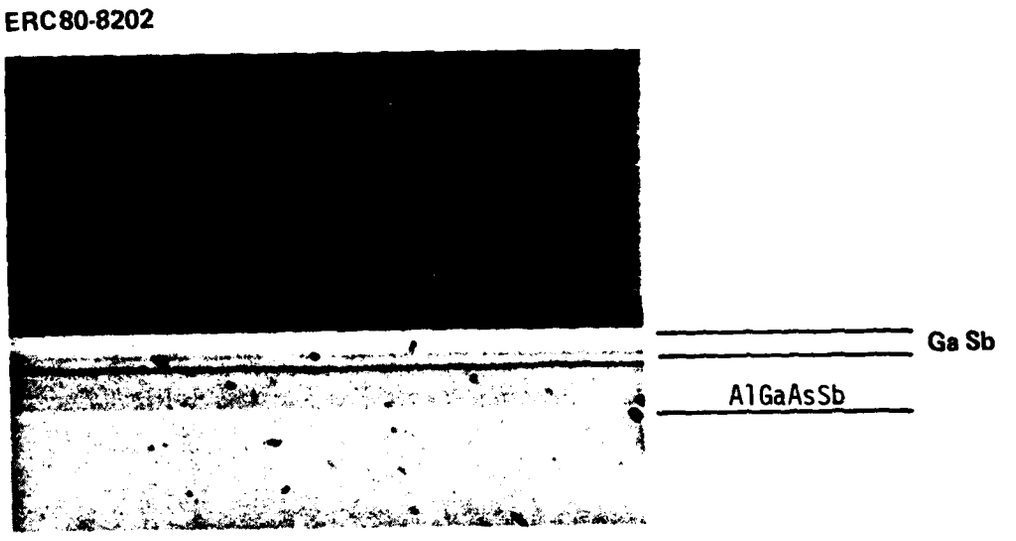

Fig. 8 Cleaved and stained cross-section of a GaSb-$Al_xGa_{1-x}As_ySb_{1-y}$ ($x = 0.3, y < 0.01$) structure. The uniform deposition of a GaSb n^+-layer onto the AlGaAsSb layer is clearly evident.

ERC80-8199

Fig. 9 Photograph of the as-grown surface of the wafer whose cross-section is shown in Fig. 8.

3.0 SCHOTTKY BARRIERS TO AlGaAsSb

The design of a process for the fabrication of Schottky gate CCDs necessitated a detailed study of Schottky barriers on AlGaAsSb. The optimum Schottky diode must have a high barrier height, nearly unity ideality factor, and low reverse leakage current. Furthermore, the metal used to form the barrier must be process-compatible, e.g., thermally stable and reasonably brittle. Thermal stability is required if the gate diode is to maintain its characteristics during subsequent processing steps. Brittleness is a desirable characteristic since the CCD gates are defined using a lift-off technique. Schottky diodes were fabricated using several different metals. The barrier height, ideality factor and reverse I-V characteristics were examined as a function of the Al mole fraction in the solid with particular emphasis on the range $0.3 \leq X_{Al} \leq 0.65$. The results of this study indicate that Cr is the best choice for a barrier metal since it is most thermally stable. This investigation has also provided useful information about the properties of the epitaxial material.

Initial attempts to fabricate discrete, guarded Schottky diodes on $Al_xGa_{1-x}As_{1-y}Sb_y$ proved to be quite problematic. Several sets of guarded dioes were fabricated using the standard CCD Schottky metallization: 500Å Cr-500Å Au. This metallization has produced very low leakage current diodes in $Al_xGa_{1-x}As$. However, the diodes on the quaternary material were found to be rather leaky and very pressure sensitive. The I-V characteristics were measured by probing the devices while still in wafer form. A probe pressure sufficient to make stable contact to the device caused a change from rectifying to ohmic behavior after several seconds of operation. New Schottky diodes were fabricated on n-epilayers grown on n^+ GaSb substrates. Three wafers with x = 0.3, 0.45 and 0.65 were used. Schottky barriers were formed by electron beam evaporation through a shadow mask. Most of the devices had relatively thick metal layers ($\sim$3500Å) to facilitate probing; however, some diodes had semitransparent Schottky barriers so that ϕ_{Bn} could be measured using the photoresponse technique. The characteristics of the thick metal diodes were found to be very

stable when probed. Since GaSb and its alloys are very soft materials, it is necessary to cushion the probe tip in order to prevent strain-induced changes in the I-V characteristics. The thick barrier metal accommodates the strain introduced by the probe tip.

The diodes were characteized by measuring the forward and reverse I-V characteristics. Barrier height and ideality factor are determined from the forward bias data and information about traps and localized defects is obtained from the reverse bias data. In addition, ϕ_{Bn} was also determined by photoresponse measurements. Typical forward and reverse I-V data for an Au Schottky diode fabricated on $Al_{.3}Ga_{.7}As_{.01}Sb_{.99}$ are shown in Figs. 10 and 11, respectively. As shown in Fig. 10, the forward current is initially dominated by a generation-recombination mechanism (n = 1.71) for $V \leq 0.15$ V and is essentially diffusion limited (n = 1.15) for larger biases. The semiconductor surface is unpassivated, therefore it is reasonable to assume that a significant portion of the g-r current is due to leakage along the surface.

The reverse I-V characteristics shown in Fig. 11 exhibit the expected g-r dependence for $V < 5$ V and show an abrupt increase for larger applied biases. Recent experiments on InP avalanche photodiodes[1] have demonstrated that this behavior is characteristics of microplasmas located in the growth striations. The sources of the microplasmas are recombination centers. The morphology of the quaternary layers used in these experiments is characterized by similar striations and, although detailed experiments have not been carried out, it is assumed that microplasmas are present here also.

By extrapolating the diffusion limited current in Fig. 10 to the current axis intercept, the barrier height can be calculated using the expression:

$$\phi_{Bn} = (kT/q)\ln(AA^{**}T^2/I_s) \qquad (1)$$

where A is the diode area, $A^{**} = 120\ m^*/m_o$ is the modified Richardson constant, T is the temperature and I_s is the forward saturation current. The effective mass of the quaternary alloy was estimated from a Veglard's law approximation for the ternary alloy $Al_xGa_{1-x}Sb$. These values should be reasonably accurate

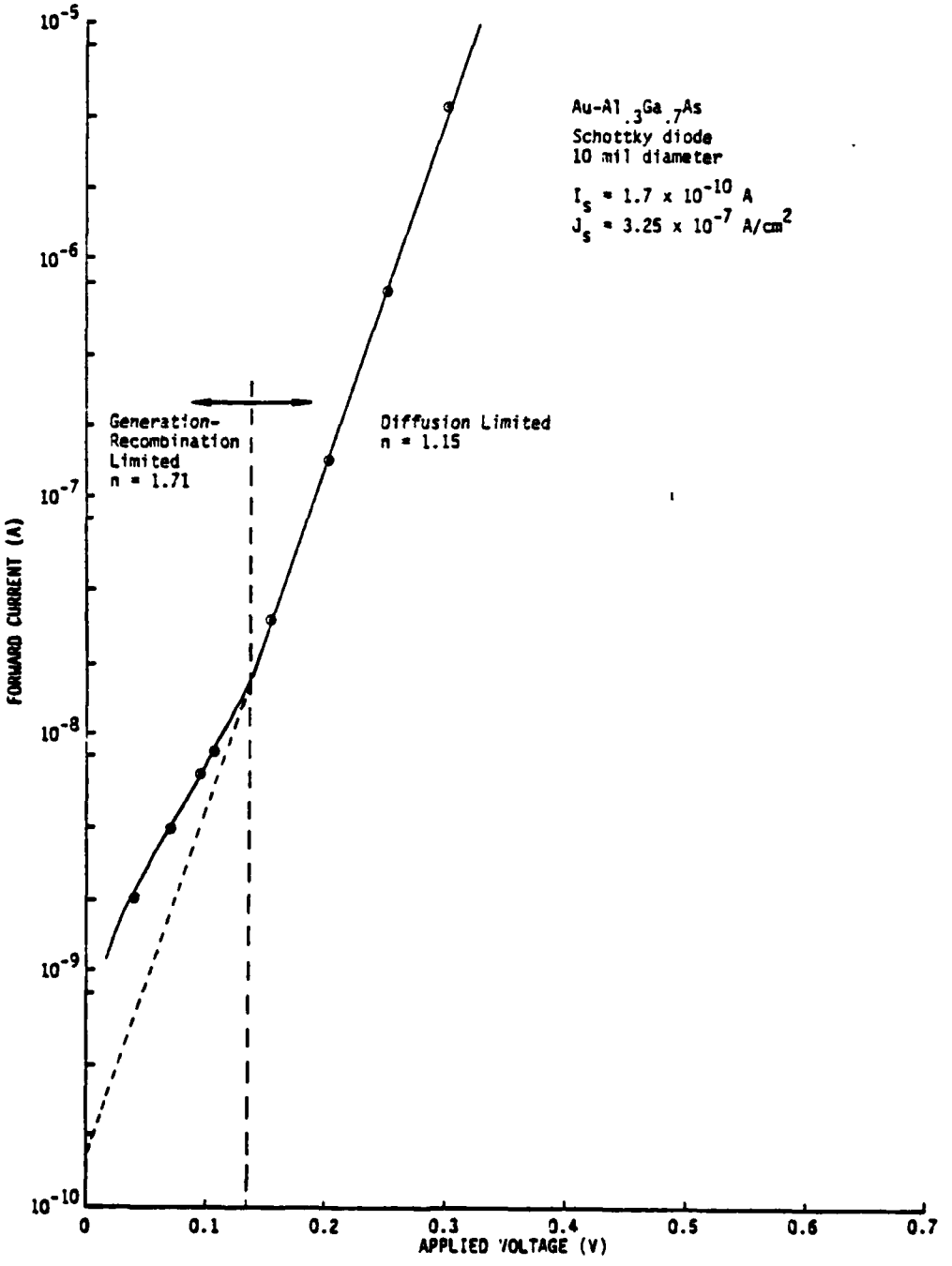

Fig. 10. Forward I-V characteristics of a Au-Al $_{.3}$Ga $_{.7}$As $_{.01}$Sb $_{.99}$ Schottky barrier diode.

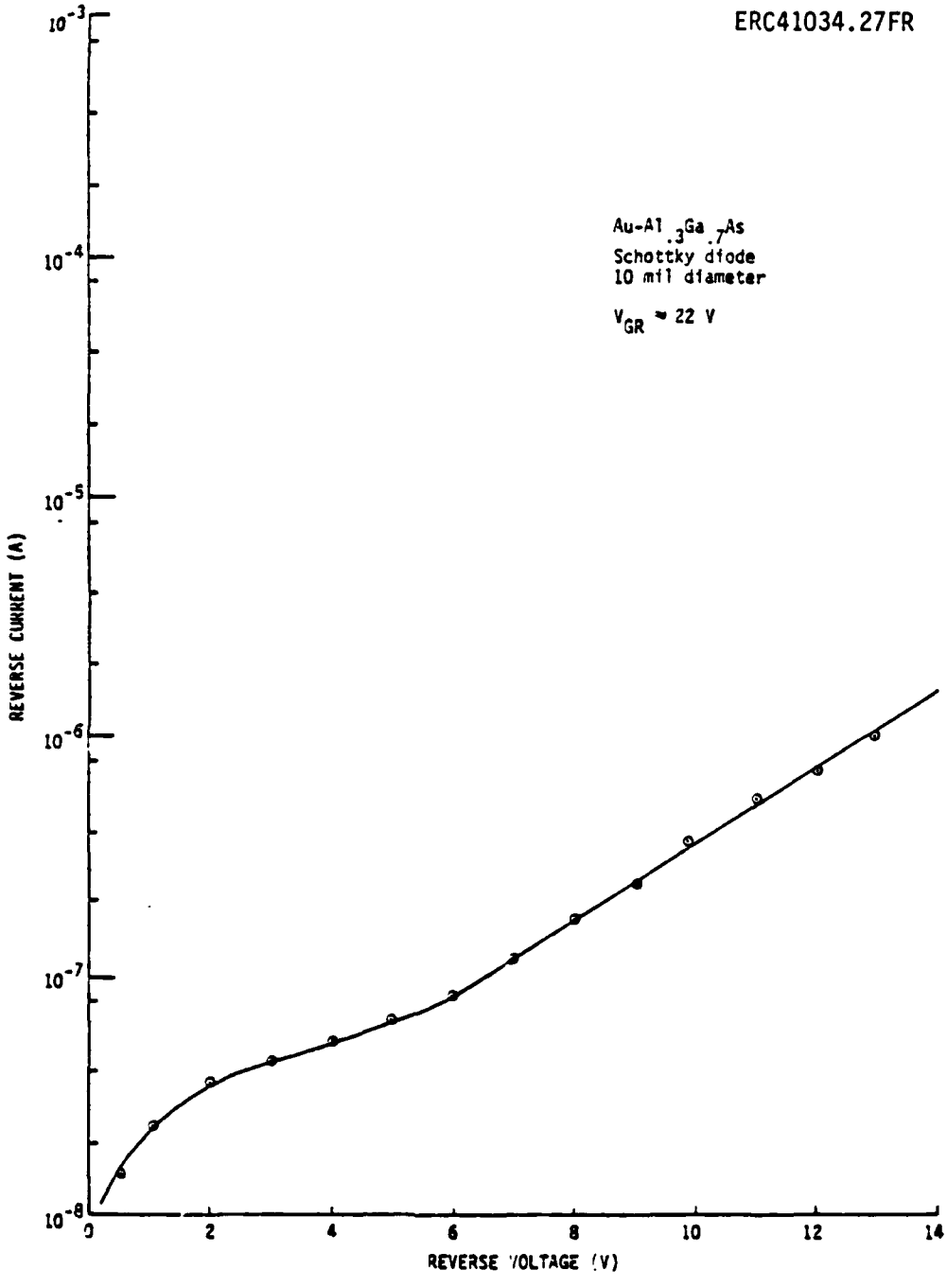

Fig. 11. Reverse I-V characteristics of a Au-$Al_{.3}Ga_{.7}As_{.01}Sb_{.99}$ Schottky barrier diode.

since very little As is contained in the solid. Photoresponse measurements of ϕ_{Bn} were also used to corroborate these data. The results of these measurements are shown in Fig. 12. Data for $x<0.3$ were taken on samples provided by H. D. Law. A difference of ~5-10% exists between the data obtained by the two methods. This is probably owing to the uncertainty introduced when the data are extrapolated to determine I_s. The average barrier height and n factor for $x>0.3$ are listed in Table 1. The alloy has an indirect bandgap for $x>0.3$, and the magnitude of the energy gap has a weaker dependence on x in this region, therefore the small variation of ϕ_{Bn} over this composition range is not surprising. The dependence of ϕ_{Bn} on X_{Al} does not agree with the "common anion" rule and is sensitive to the Ga/Al cation ratio. This topic is explored more fully in a recent publication[2]. The measured values of ϕ_{Bn} and n indicate that if the surface contribution to the total leakage current can be controlled, sufficiently low dark current CCD gates can be fabricated.

The results presented above demonstrate that low leakage current Schottky barriers can be formed on AlGaAsSb by e-beam evaporation. This technique, however, is not directly applicable to the fabrication of guard ring isolated CCDs. The current intermetallic insulator technology employed in the fabrication process utilizes plasma-deposited Si_3N_4 which requires that the Schottky barrier be held at 250°C for 30 min. during deposition. Since Au rapidly diffuses into the alloy at temperatures above 100°C, the Schottky barrier characteristics are permanently degraded and are useless as CCD gates.

Three alternative barrier metals, Cr, Ni and Ti, have been examined as possible substitutes. Schottky diodes were fabricated on $Al_{.3}Ga_{.7}As_{.01}Sb_{.99}$ by e-beam evaporation through a shadow mask. The metal films were 2000Å thick. The I-V characteristics of the diodes were measured after fabrication and subsequent to annealing at 150°C and 225°C for 30 min. The barrier heights and ideality factors are presented in Table 2. Each table entry is the average of more than five data points. Both Ni and Ti exhibit degraded characteristics after annealing. The decrease in ϕ_{Bn} and corresponding increase in ideality factor indicate that the character of the metal-semiconductor interface is significantly altered. The high n values imply the enhancement of generation-

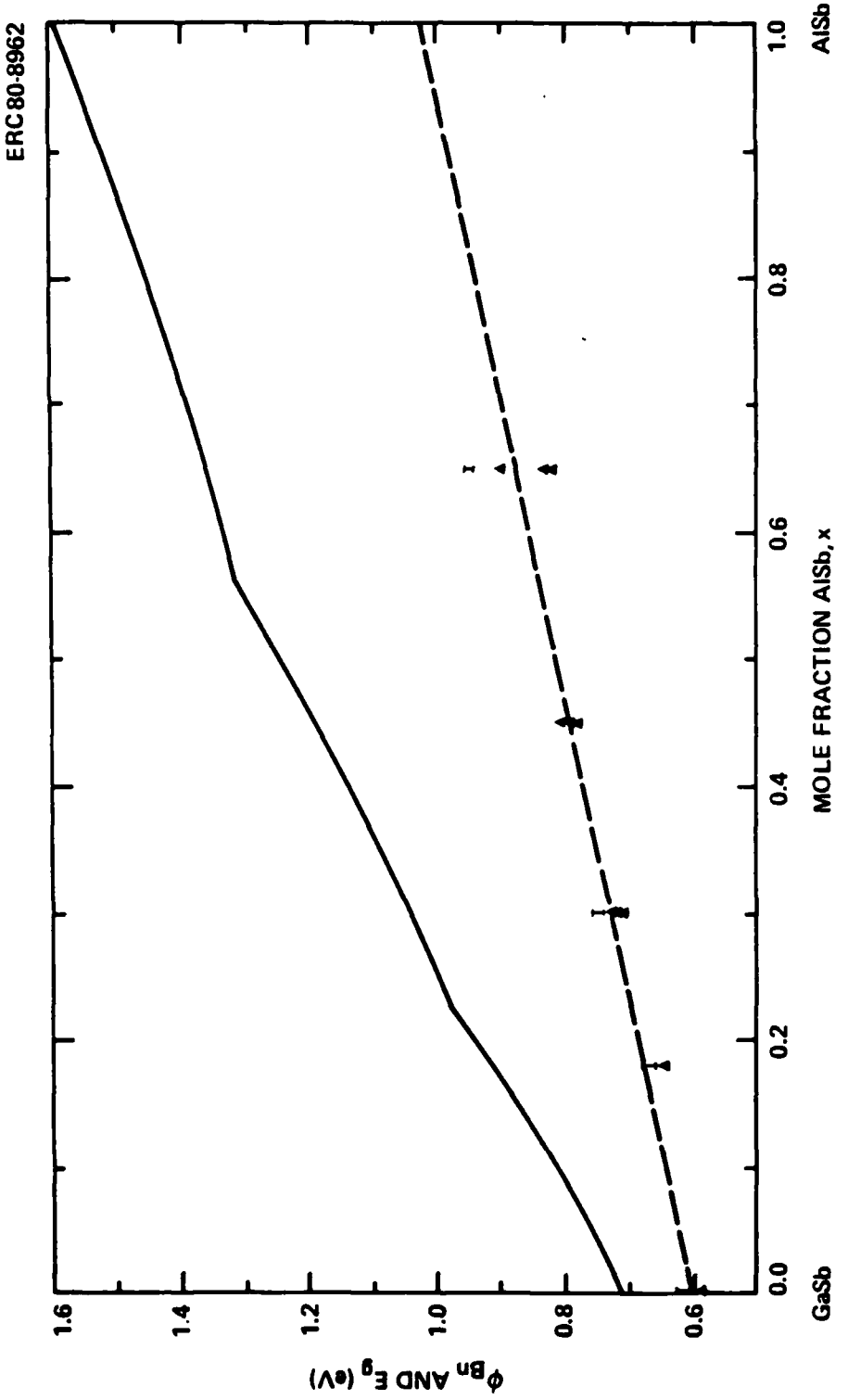

Fig. 12. Au Schottky barrier height and energy gap vs. Al mole fraction. The I-V data are denoted by Δ and the spread in photoresponse data are denoted by vertical bars.

TABLE 1

BARRIER HEIGHT AND IDEALITY FACTOR OF Au SCHOTTKY DIODES FABRICATED ON $Al_xGa_{1-x}Sb_{1-y}As_y$

x	ϕ_{Bn} (eV)	n
0.3	0.73	1.3
0.45	0.79	1.2
0.65	0.83	1.3

TABLE 2

TEMPERATURE DEPENDENCE OF THE BARRIER HEIGHTS AND IDEALITY FACTORS OF Cr, Ni AND Ti BARRIERS FABRICATED ON $Al_{.3}Ga_{.7}As_{.01}Sb_{.99}$

	As-Fabricated		150°C Anneal		225°C Anneal	
	ϕ_{Bn} (V)	n	ϕ_{Bn} (V)	n	ϕ_{Bn} (V)	n
Cr	0.704	1.12	0.697	1.11	0.712	1.23
Ni	0.744	1.19	0.709	1.37	0.699	1.45
Ti	0.715	1.09	0.713	1.23	0.692	1.48

Consideration of the results presented above clearly shows that Cr is the optimum metal for Schottky barrier formation on AlGaAsSb. The barrier height is comparable to that obtained using Au as the barrier metal. (ϕ_{Bn}(Au) is considered to be the upper limit on the value ϕ_{Bn} since Au is one of the most electronegative metals) In addition, the dark current of a Cr-$Al_{0.3}Ga_{0.7}As_{0.89}Sb$ Schottky barrier (ϕ_{Bn}= 0.074V) is ~ 5 x 10^{-13} A/cm^2 at 200°K which is much less than the channel generation current. Cr Schottky barriers are thermally stable at room temperatures normally encountered in the CCD processing sequency. Also, Cr is a very brittle metal and, therefore, excellent gate and gap definition can be achieved using a lift-off procedure.

recombination mechanisms. Since it is known that Ni does not diffuse very far into AlGaAsSb (see Section 4, ohmic contacts), the mechanism for this enhancement is probably the production of traps by the out-diffusion of As and Sb. In contrast, the barrier height and ideality factor of the Cr Schottky diodes remains nearly constant. Apparently Cr successfully prevents out-diffusion of the column V elements. Therefore, the metal-semiconductor interface remains relatively stable.

4.0 OHMIC CONTACTS

The standard procedure for the formation of ohmic contacts to AlGaAsSb is to alloy a multilayer thin film of Au-Ge/Pt/Au. The alloy temperature is typically in the range 270-330°C. Good ohmic contacts can be achieved using this technique; however, Au rapidly diffuses into the material. This technique is not useful for the fabrication of ohmic contacts to a CCD channel layer because the contact constituents diffuse through this relatively thin (1 μm) layer and short out the underlying heterojunction. An Auger analysis of an alloyed AuGe/Pt/Au contact region is shown in Fig. 13. The Al peak defines the position of the quaternary channel layer. The Pt diffusion barrier is ineffectual in preventing the penetration of Au into the GaSb substrate.

Several new contacting schemes have been investigated including (1, the formation of shallow n^+ regions by ion implantation, (2) ion bombardment of AuGe, and (3) the use of low temperature eutectics which do not contain Au. The common theme linking these choices is the search for a substitute for the fast diffusing Au in the contact recipe. Only partial success was achieved with methods (1) and (2). Se was chosen as the n^+ implant species, and fair ohmic contacts were formed as shown in Fig. 14; however, the underlying heterojunction was shorted by the implant anneal. Since Se is known to remain localized near the surface of AlGaSb, diffusion of implant generated defects is suspected as the cause of junction degradation.

Bombardment of AuGe films by ions was used in an attempt to drive the contact constituents into the material without the need for a thermal annealing. Kr was selected as the ion since the peak of the Gaussian distribution would be close to the metal-semiconductor interface for a 300 keV implant. Ohmic contacts can be formed using this technique; however, they are of variable quality and often irreproducible. A common problem with even the best bomarded contacts an example of which is shown in Fig. 15, is high resistance. This is most likely due to the residual damage from the unannealed implanted region.

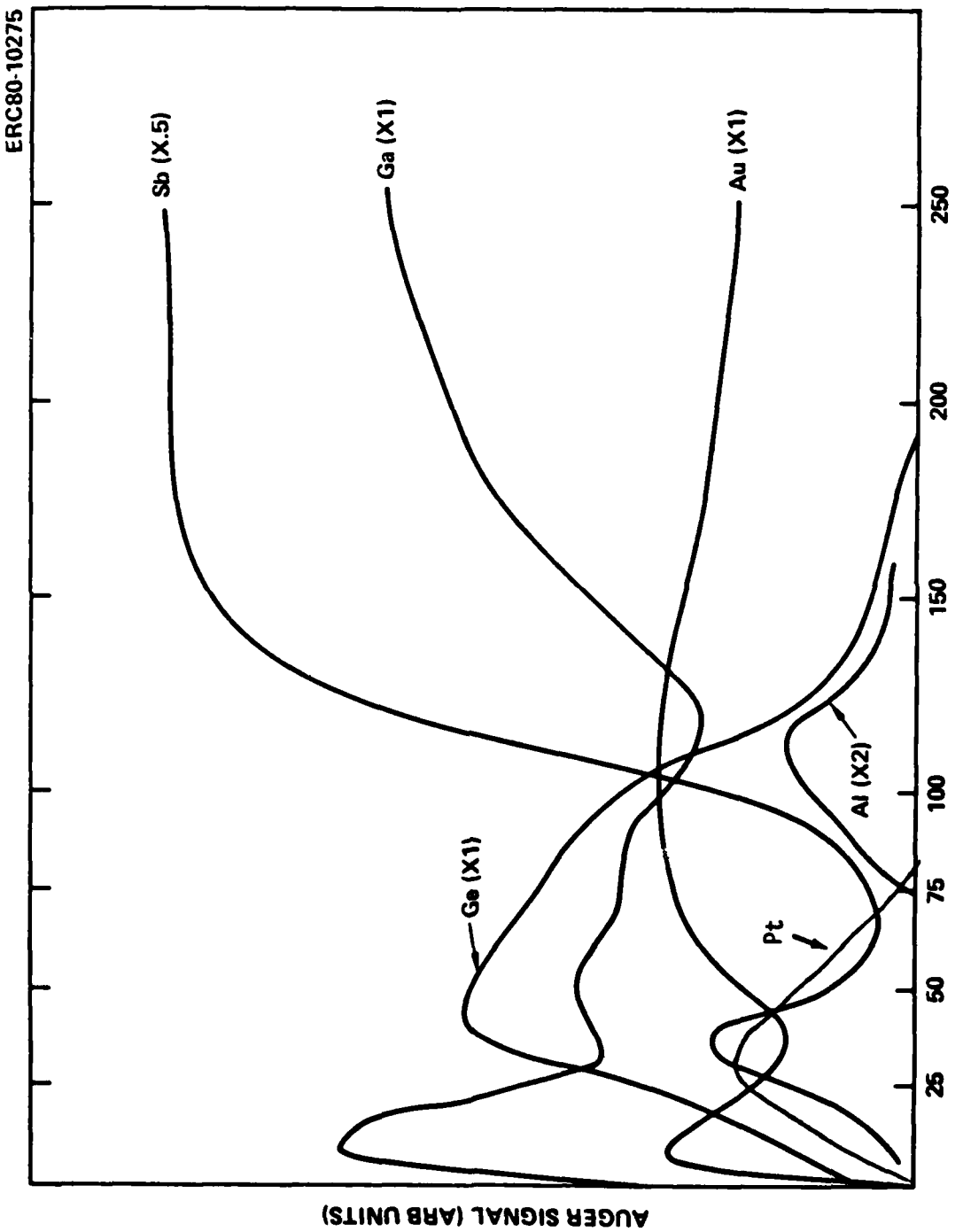

Fig. 13. Depth composition profile for AuGe/Pt/Au metallization determined by AES.

ERC80-7262

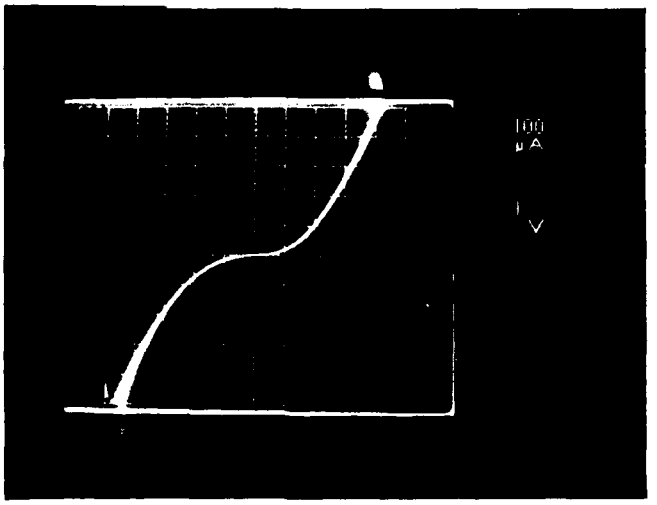

(a)

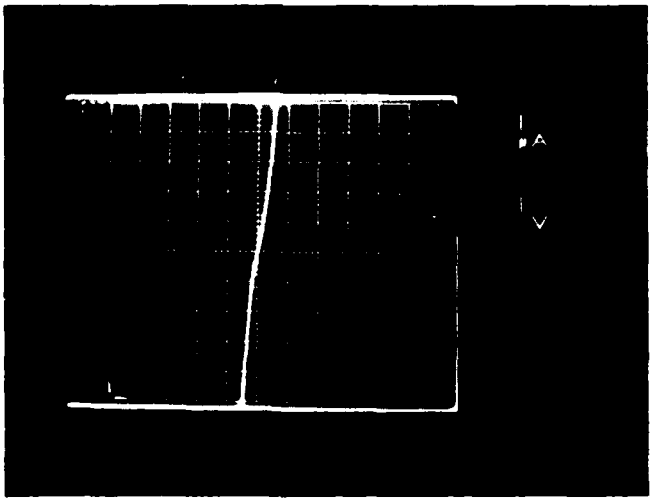

(b)

Fig. 14 (a) I-V characteristics of aluminum contacts on n-$Al_{.3}Ga_{.7}AsSb$/p-GaSb (wafer K108d) after 200 KeV Se implant at 1 x $10^{13}cm^{-2}$ dosage, (b) at lower current scale.

ERC80-7349

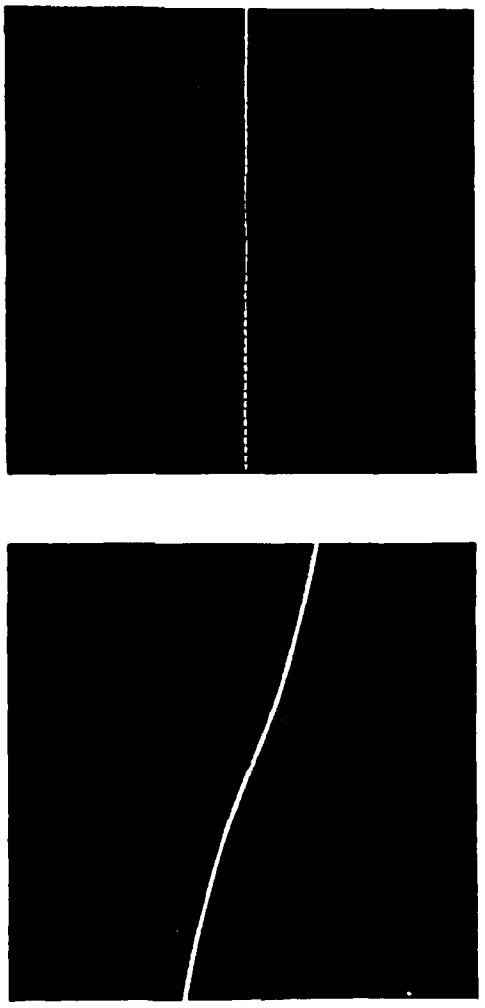

Fig. 15 Sample K108g, ohmic metal - 400Å Ge/240Å Au, implant - Kr^{+} - 300 KeV, 1 x 10^{14}ions/cm^2, post implant anneal - none.

The successful fabrication of ohmic contacts using Au-Ge demonstrated that evaporated metal eutectics provide a simple means of contact formation. The use of Au-based eutectics for the contacting of material containing significant amounts of Al is not an optimized technique since Au and Al are essentially insoluble. Therefore, group III vacancies can be generated only when Au reacts with the Ga in the semiconductor. In order to eliminate this problem, a Ag-based eutectic was used to contact the AlGaAsSb. Ag combines with both Al and Ga, therefore significantly more vacancies are formed which can accomodate dopant atoms.

Ohmic contacts were formed by sequentially evaporating 100Å Sn/200Å Ag/500Å Ni onto $Al_{.3}Ga_{.7}As_{.01}Sb_{.99}$. Circular contact areas of differing dimensions were defined photolithographically prior to evaporation. The sample was cleaved into nine pieces and each piece was alloyed for 5 min. An alloy temperature range of 275-475°C was investigated in 25°C increments. The I-V characteristics between dots with varying center-to-center spacings were examined on a curve tracer. Samples that were alloyed at 350°C had nonlinear I-V characteristics and the resistance uniformity was very poor. For alloy temperatures $\geq$375°C, the uniformity and linearity improved significantly with the best results in the 400-425°C range. A typical I-V characteristic of Sn/Ag/Ni contacts alloyed at 425°C is shown in Fig. 16. The total resistance measured between the contacts is independent of contact separation indicating that the resistance of the contact dominates the measurement. The total resistance is shown as a function of alloy temperature in Fig. 17. Specific contacts resistance was calculated using the expression $R_c = (R_T/2)A$, where R_T is the total measured resistance between the contacts and A is the contact area[3]. The minimum R_c was obtained for an alloy temperature of 425°C. At this temperature, $R_c \leq 1.3 \times 10^{-3} \Omega\text{-cm}^2$.

The results of the AES analysis of the contacts alloyed at 375°C and 475°C are shown in Figs. 18 and 19, respectively. At 375°C, Ag remains localized in a region very near the surface of the semiconductor. Only a small amount of Sn has penetrated into the material. The relative positions of the Ag and Sn peaks indicate that at this temperature Sn is moving into the Ni cap layer

ERC80-9541

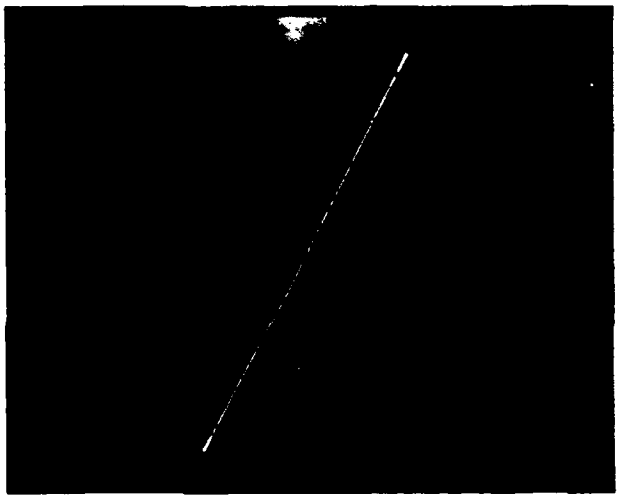

Fig. 16 I-V characteristics of Sn/Ag/Ni metallization after 425°C alloy. Vertical scale: 20 mA/div; Horizontal scale: 0.5 V/div.

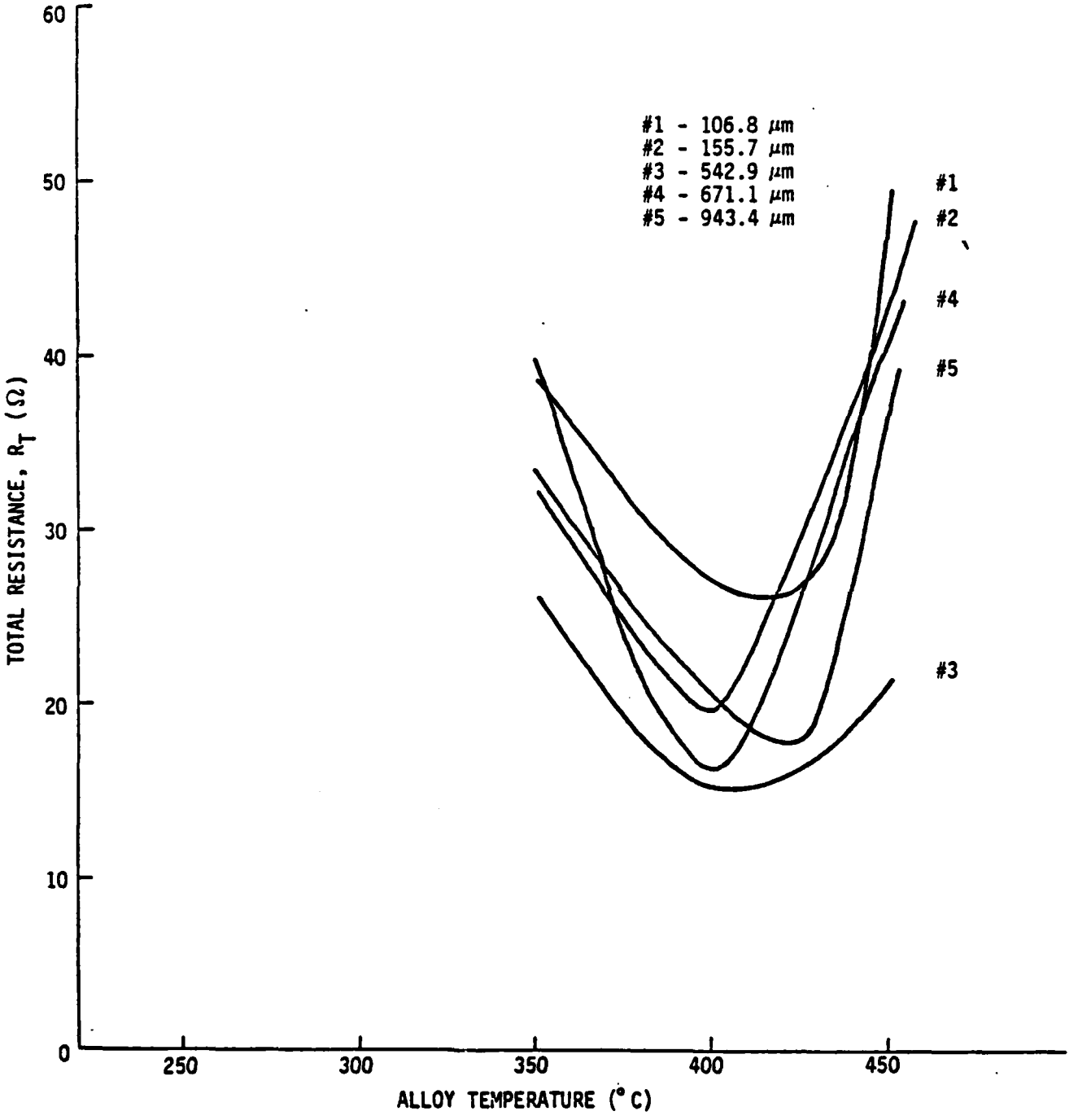

Fig. 17. Total resistance vs. alloy temperature of Ag-Sn-Ni metallization system on n-$Al_{.3}Ga_{.7}As_{.01}Sb_{.99}$. The contact areas are circular, having the diameters listed in the figure.

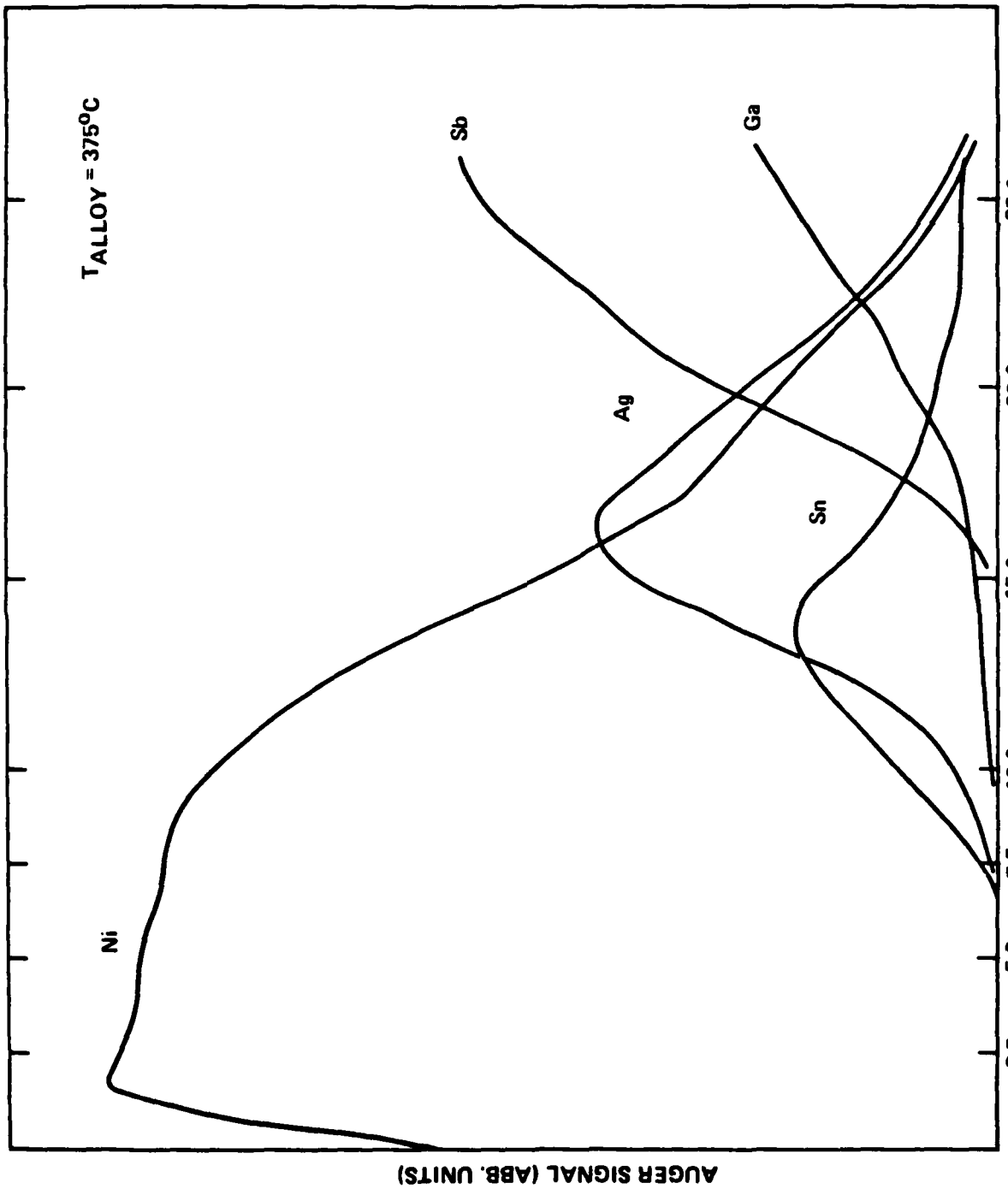

Fig. 18. Depth composition profile for Sn/Ag/Ni metallization determined by AES. The data for all elements are X1. Al data have been deleted for clarity. (For both 375°C, 475°C, Auger signal for Al didn't become sizable until ~ 24 min of sputtering time. Very little data available, therefore not included.)

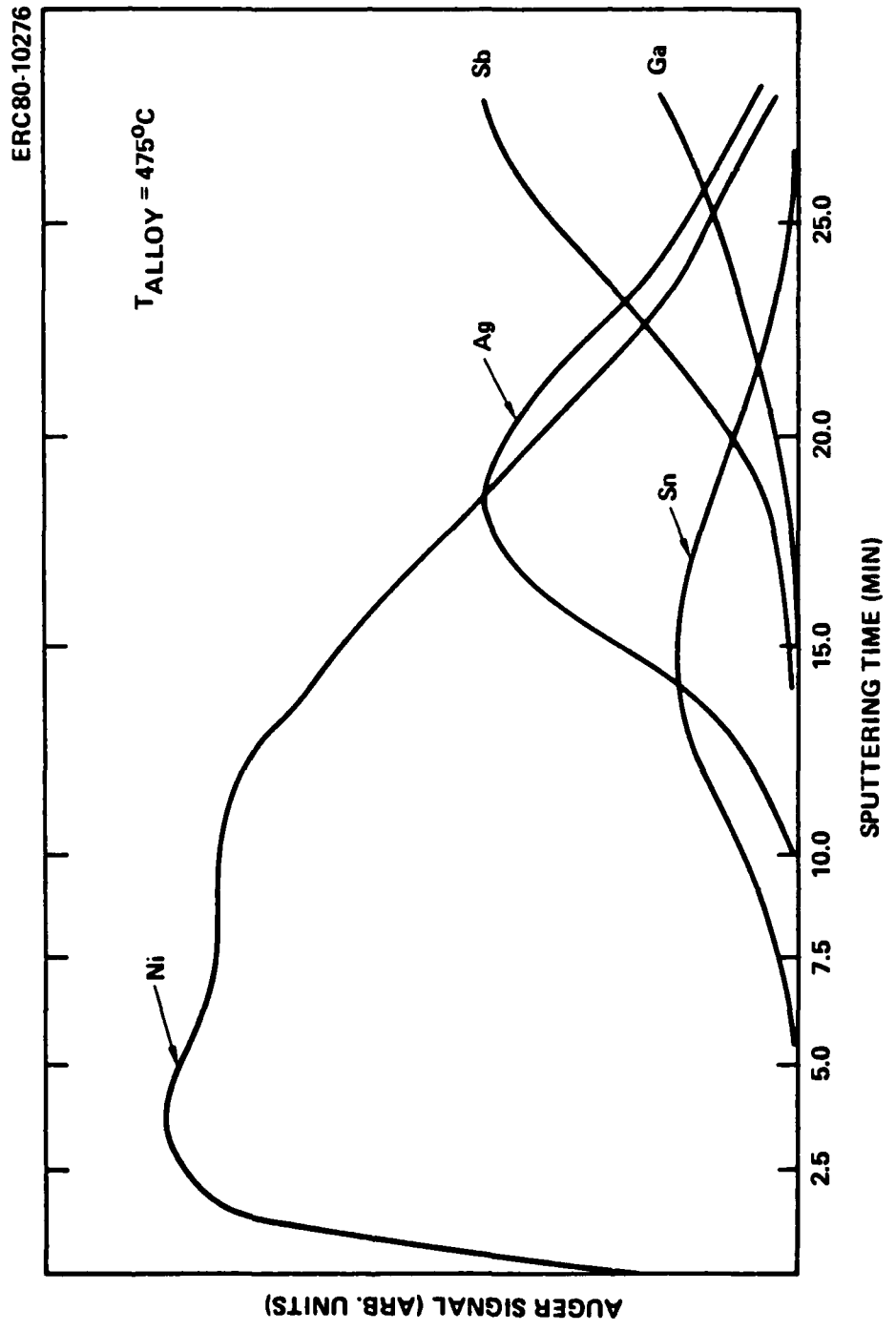

Fig. 19. Depth composition profile for Sn/Ag/Ni metallization determined by AES. The data for all elements is X1. Al data have been deleted for clarity.

layer. Alloying at 475°C produces a somewhat broader interface region; however, relatively locations of Ag and Sn and the depth of penetration of each into the semiconductor is essentially unchanged. A Ni cap was originally chosen to prevent the contact metals from balling up for T>229°C (eutectic temperature of Ag-Sn). As shown in Figs. 18 and 19, it effectively stops the outdiffusion of Ga and Sb from the semiconductor. Very few vacancy sites are therefore available for the dopant atoms to occupy, consequently the contact resistance of this system is relatively high.

5.0 PROCESSING ISSUES

In the preceding sections, the epitaxial growth of GaSb and AlGaAsSb, the fabrication of low leakage, thermally stable Schottky barriers, and a reliable ohmic contact formula for AlGaAsSb have been described. However, no CCDs have, as yet, been produced. The major roadblock to the fabrication of devices is the lack of suitable etchants, both selective and non-selective. This problem was not anticipated based on information available at the start of this program. The results to date indicate that it is related to the surface chemistry of the GaSb-AlGaAsSb materials system.

Wet chemical etchants are required for a variety of processing functions. The fabrication of a glass bonded imaging CCD requires the removal of the substrate after the material has been attached to the glass window. This is usually accomplished by a material selective etchant which can distinguish moderate differences in Al content. Non-selective etches are used during processing to remove contaminants from the surface of the material. The major requirements of an etching solution for use in semiconductor processing are (1) slow to moderate etch rate ($\leq$10,000Å/min), (2) uniform etching over wafer surface, and (3) no residual etchant by-product deposition on the material. Etch rates $>$10,000Å/min present problems in wafer handling while non-uniform etching destroys the planarity of the surface, making photoprocessing impossible. Reactant products of the etch components and the material, in the form of opaque films on crystallites, can change the character of the surface. These contaminants must be removed before processing can continue, and, even if removed, the electrical properties of the surface may be permanently changed.

Etching experiments were performed on LPE-grown GaSb and $Al_{.3}Ga_{.7}Sb$ layers, and the results are shown in Table 3. The majority of etchants acted much too quickly and left opaque deposits on the surface of the material. Only two solutions, neither of which is material selective, were found useful for etching GaSb: 10 H_2O:1 H_3PO_4:1 H_2O_2 and 20 H_2O:1 HF. The dilute HF solution is the more useful since it is well-controlled with an etch rate of 400Å/min.

TABLE 3

ETCHANT	GaSb	$Al_{.3}Ga_{.7}As_{.01}Sb_{.99}$	COMMENTS
5 H_2O:1 H_3PO_4:1 H_2O_2	5,000Å/min	7,000Å/min	Occasional formation of black crystallites in etched area.
10 H_2O:1 H_3PO_4:1 H_2O_2	2,500Å/min		Clean etch (no discoloration) on the one sample tried.
5 H_2O:1 H_2SO_4:1 H_2O_2	45,000Å/min	51,000Å/min	A thin cracked film covered etched area which was not removed in HF or HCl.
10 H_2O:1 H_2SO_4:1 H_2O_2	29,000Å/min		A thick cracked film covered etched area which was not removed in HF or HCl
H_2O_2 adjusted to a pH of 7.1 with NH_4OH (superoxol)	No etch		
10 H_2O:1 NH_4OH:1 H_2O_2	400Å/min to less than 20Å/min	No apparent etch	GaSb: Clean etch - no discoloration. *Etch rate not reproducible.* $Al_{.3}Ga_{.7}Sb$: very discolored surface.
20 H_2O:1 HF	400Å/min		Clean etch - no discoloration
10 H_2O:1 HF:1 H_2O_2		>100,000Å/min	Clean etch - no discoloration
100 H_2O:1 HF:1 H_2O_2		15,000Å/min	Surface very discolored.
10 H_2O:1 Buffered HF (10:1):1 H_2O_2		30,000Å/min	Clean etch - no discoloration
20 H_2O:1 Buffered HF (10:1):1 H_2O_2		17,000Å/min	Some surface discoloration
20 Acetic Acid:9 HNO_3:1.5 HF		>50,000Å/min	Uneven etch, dense striations in some areas with thick cracked film in others
120 Acetic Acid:9 HNO_3:1.5 HF		20,000Å/min	Uneven etch, with decrease in areas covered by striation and an increase in areas covered by thick cracked film as compared to above sample.
Br-Methanol	Variable	Variable	No control over etch rate.
Br_2/HBr	Variable	Variable	Etched surface is very uneven.

NOTE: Etch rates determined from Dektak measurements.

No completely satisfactory etchant has been found for the quaternary alloy. Dilute solutions of HF and H_2O_2 leave no residue on the surface; however, the etch rates are much too high to be of practical use. Attempts to reduce the etch rate by increasing the dilution factor resulted in the formation of residual deposits on the wafer surface. It is suspected that a complexing agent, added to the etchant, will produce the required etch rate without any residues; however, lack of time did not permit further experimentation.

Material selective etches which can distinguish moderate differences in Al concentration have been developed for the GaAs-AlGaAs materials system. Several of these etches have been applied to the GaSb-AlGaAsSb system, without success. In all cases, the etches fail to distinguish any differences between the material. The failure of these solutions to perform the desired function is apparently associated with the Sb content of the surface. In fact, the variable etch rates of even the non-selective etches are probably also related to the amount of Sb. In order to develop a selective etchant suitable for this alloy system, a systematic study of the surface chemistry must be initiated. Of particular importance is the amount of Sb present at the surface and how various processing techniques change this amount. With this information, it will be possible to design redox systems[4] to accomplish selective etching in a well-controlled fashion.

6.0 CONCLUSIONS AND RECOMMENDATIONS

Several major accomplishments have resulted from our efforts to fabricate Schottky gate, imaging charge coupled devices in the AlGaAsSb alloy system. The growth of alloys containing 30-65% Al has been investigated in detail and a technique has been developed for the growth of GaSb on $Al_xGa_{1-x}As_{1-y}Sb_y$ with $x>0.3$. A reproducible ohmic contact technology for lightly doped AlGaAsSb, using alloyed Ag/Sn/Ni thin films, has also been demonstrated. At the start of the program, these were unsolved problems of major importance. In addition, a thermally stable Schottky gate metal has been identified which is well suited to photolithographic processing. These developments represent the key elements necessary for the realization of imaging CCDs.

The most significant problem area which remains is that of device fabrication, including the development of surface passivants, etchants, and "process recipes". Our present techniques, based on GaAs technology, have proven inadequate. Some progress has been made in understanding the surface chemistry of the material. The investigation of etchant-alloy interaction, described in Section 5.0, also indicates that the wafer treatment history is of great importance. The effects, if any, of photolithographic chemicals, e.g., resists, developers, on the surface properties are, at this time, unknown. This is also true of the available passivation materials. A detailed investigation of these areas must be made in order to increase the probability of fabricating complex devices in this material system.

It is clear from the work presented here that the GaSb-AlGaAsSb material system is well suited to night vision applications and that significant progress has been made in understanding the characteristics of fundamental device building blocks. It is also apparent, however, that the material is significantly different from the more well-understood III-V compounds, such as GaAs, and requires the development of specialized techniques. Because of the magnitude of this difference, a research and development program in process-development is required. This program should include: (a) the development of etchants, both selective

and non-selective, (b) an investigation of the effects of dry processing techniques, e.g., plasma etching and (c) the development of surface passivation techniques. These results, coupled with the achievements of the present program, will provide all of the building blocks necessary for the realization of a wide class of devices.

REFERENCES

1. F. Capasso, P. M. Petroff, W. L. Bonner and S. Sumski, Electron Dev. Lett. EDL-1, 27 (1980).

2. Raymond Chin, R. A. Milano and H. D. Law, Elec. Lett. 16, 626 (1980).

3. M. Itoh, S. Suzuki, T. Itoh, Y. Yamamoto and K. G. Stephens, Solid State Electron. 23, 447 (1980).

4. R. P. Tyburn and T. van Dongen, J. Electrochem. Soc. 123, 687 (1976).

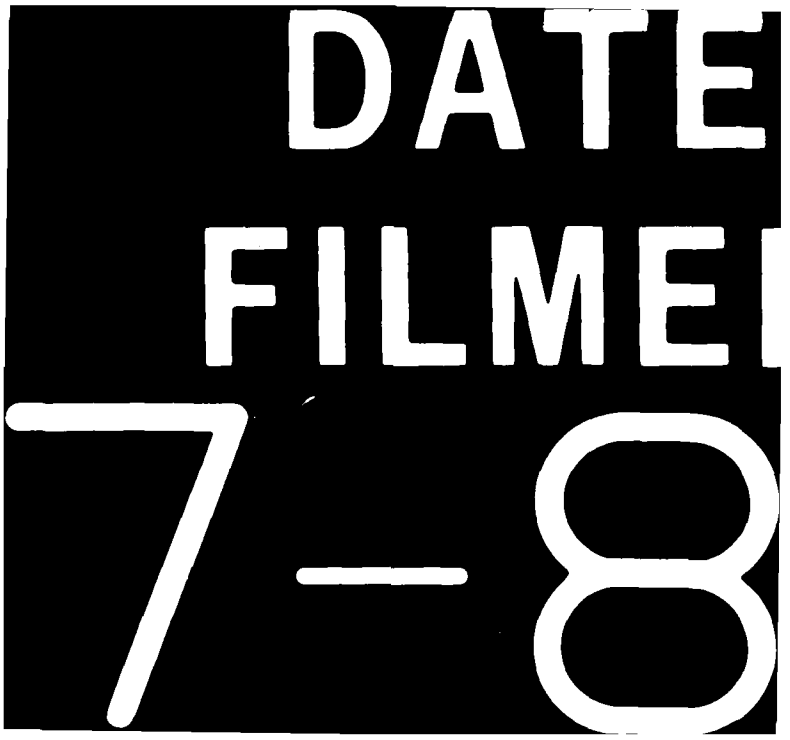
DATE
FILME
7-8